Article

Characterization of a New Microstructure in a β-Solidifying TiAl Alloy after Air-Cooling from a β Phase Field and Subsequent Tempering

Yi Chen [1], Liang Cheng [1],[*], Lingyan Sun [1], Yalin Lu [1], Guang Yang [2], Hongchao Kou [3] and Emmanuel Bouzy [4]

[1] School of Materials and Engineering, Jiangsu University of Technology, Changzhou 710072, China; chenyi@jsut.edu.cn (Y.C.); sunly@jsut.edu.cn (L.S.); luyalin@163.com (Y.L.)
[2] College of Mechanical and Electrical Engineering, Shaanxi University of Science and Technology, Xi'an 710021, China; yangguang_wxn@126.com
[3] State Key Laboratory of Solidification Processing, Northwestern Polytechnical University, Xi'an 710072, China; hchkou@nwpu.edu.cn
[4] LEM3, CNRS UMR 7239, Université de Lorraine, Ile du Saulcy, 57045 Metz CEDEX 1, France; emmanuel.bouzy@univ-lorraine.fr
[*] Correspondence: chengliang525@163.com; Tel.: +86-0519-8695-3289

Abstract: In this study, we found that well-developed α_2' martensite was formed in a Ti-40Al-10V (atomic percent or at.%) alloy after air-cooling from a β phase field, rather than the traditional α_2/γ lamellar colonies. The martensitic laths were produced according to the Burgers orientation relationship (OR), the same as those during quenching. Local variant selection detected that three (or six) α_2' variants sharing one (or two) common $[11.0]_{\alpha_2'}$ axes were predominant, while no global variant selection was observed. Subsequent to the martensitic transformation, the retained β phase was decomposed mainly via a β→γ transformation. The γ laths always nucleated at the α_2'/β interface according to a Blackburn orientation relationship. In order to stabilize the microstructure, the air-cooled samples were tempered at 800–1000 °C. During tempering, the microstructure decomposed mainly via an α_2'→γ transformation. The martensite was almost completely transformed after tempering at 1000 °C for 4 h, and hence a fine β-γ microstructure was obtained. Such a treatment resembling the quenching–tempering in steels may be a new strategy for the microstructural design of TiAl alloys, while an unexpected quenching process can be avoided.

Keywords: titanium aluminides; martensitic transformation; variant selection; microstructure; electron back-scattered diffraction

1. Introduction

The β-solidifying TiAl alloys have attracted intense attention in the last two decades due to their superior high temperature mechanical properties as well as good hot workability [1–3]. They are different from the traditional peritectic-solidifying TiAl alloys, there is a β→α transformation in the β-solidifying TiAl alloys as that in ordinary titanium alloys. The β→α transformation is of great significance for titanium alloys, because it is a critical factor in determining their microstructural morphologies and the mechanical properties [4]. The β→α transformation in titanium alloys is quite sensitive to cooling rates. When cooled from the β phase field at low or moderate cooling rates, Widmanstätten α laths precipitate mainly at β grain boundaries or grain boundary allotriomorphs and grow into β grains with orientations according to the Burgers orientation relationship (OR), leading to colony or basket-weave microstructures [4]. The retained β phase is highly enriched with β-stabilizing elements [1]. At high cooling rates a massive transformation occurs. The massive α phase

also nucleates at grain boundaries, but grows by migration of the interface without compositional variation [4]. Under very fast cooling, such as quenching, a displacive β→α′ martensitic transformation is predominant. The α′ martensite directly nucleates in the β grain interior and generally there is no grain boundary α′ plate [5].

This is quite different from conventional titanium alloys, for most β-solidifying TiAl alloys, such as high Nb-containing TiAl alloys, the transformed α phase mainly adopts a Widmannstätten morphology even under fast cooling rates [6]. The martensitic β→α transformation rarely arose and has never been noted in binary TiAl alloys even after ice-brine quenching [7], probably due to the ultra-high β→α transus, which promotes the massive transformation [1]. Only in several special cases can the martensitic transformation be detected. For instance, Hu and Jiang [8] have noted lenticular martensite with midribs in a Ti-44Al-4Nb-4Hf-0.1Si alloy, but they only form under ice-brine quenching and are accompanied by massive α_2 plates. Mayer et al. [9] have detected β→α_2′ martensitic transformation in a Ti-44.58Al-3.23Mo-0.12B alloy water-quenched from the β phase field, but the obtained lath martensite was very fine and slender, and its thickness was only ~0.1 μm, which was quite difficult analyze using electron microscopy.

Given this situation, one can note that the martensite is very difficult to initiate in β-solidifying TiAl alloys. However, as pointed by Appel et al. [10], the propensity of the β phase to undergo a martensitic transformation could be used to design specific microstructures for TiAl alloys. This requires not only a comprehensive understanding of martensitic morphology and crystallography, but also of the increasing tendency of the alloys to undergo a β→α_2′ martensitic transformation. According to the work by Takeyama and Kobayashi [11], a rising content of V elements and reduced Al content in the Ti-Al-V system would result in a remarkable variation of the β-decomposition mechanism from the massive to martensitic mode during quenching. One may speculate that if the V additions are sufficiently high (combined with a low Al content), a martensitic transformation may be expected even under moderate cooling rates. To examine this point, in this study a Ti-40Al-10V (at. % hereafter) alloy was adopted to characterize the microstructure after air-cooling from the β phase field, as well as the microstructural evolution during the subsequent tempering. The resultant microstructure was analyzed in detail using electron back-scattered diffraction (EBSD).

2. Materials and Methods

A 15 kg TiAl ingot with a practical composition of Ti-38.89Al-9.62V was prepared by vacuum arc re-melting followed by induction skull melting. Cylindrical samples with a dimension of $\Phi 20 \times 25$ mm^2 were cut from the ingot and annealed at 1350 °C (i.e., in the single β phase field) for 20 min, followed by air-cooling (AC) to room temperature. For comparison, the samples were also brine-quenched (QC) from β phase field. To avoid the decomposition of the β phase during transfer from the furnace, the transferring time was limited to less than 2 s. After that, the samples were sectioned at 1/3 of the length from the end. The cross-section was mechanically polished for microstructural characterization. In order to obtain a stabilized microstructure, the AC samples were tempered at 800–1000 °C. After that, the microstructures of all the samples (QC, AC and tempering samples) were examined by using electron back-scattered diffraction (EBSD) (Oxford Instruments, Oxford, UK) with step sizes of 50–200 nm conducted on a Zeiss-∑IGMA500 scanning electron microscope (Carl Zeiss AG, Oberkochen, Germany). It should be pointed out that because of the slight tetragonality ($c/a \approx 1.02$) of the γ lattice, it is quite difficult identify by EBSD [12]; in the present study it was treated as normal face-centered cubic (FCC) lattice instead. The EBSD data was analyzed by using the HKL Channel 5 software (Oxford Instruments, Oxford, UK). Before that, noise reduction was preformed so that the "wild spikes" were removed. An energy dispersive spectrometer (EDS) (Oxford Instruments, Oxford, UK) was also performed to reveal the compositional deviation among various constituent phases.

3. Results and Discussion

3.1. Phase Constituents and Morphology

The microstructure of the Ti-40Al-10V alloy after QC is shown in Figure 1. The optical microscopic image (Carl Zeiss AG, Oberkochen, Germany) demonstrates that the microstructure mainly consists of large β (actually it is in B2 ordered form, hereinafter we use β to denote both the β and B2 phase) grains with a size of 3–5 mm. However, in the β grain interior about 65 vol. % of the matrix has transformed into α_2' martensitic laths as shown in Figure 1b. No composition variation was detected by EDS. This is not surprising, because under such conditions (brine-quenching), martensitic transformation is predominant for the alloy with such low-Al and high-V contents [7].
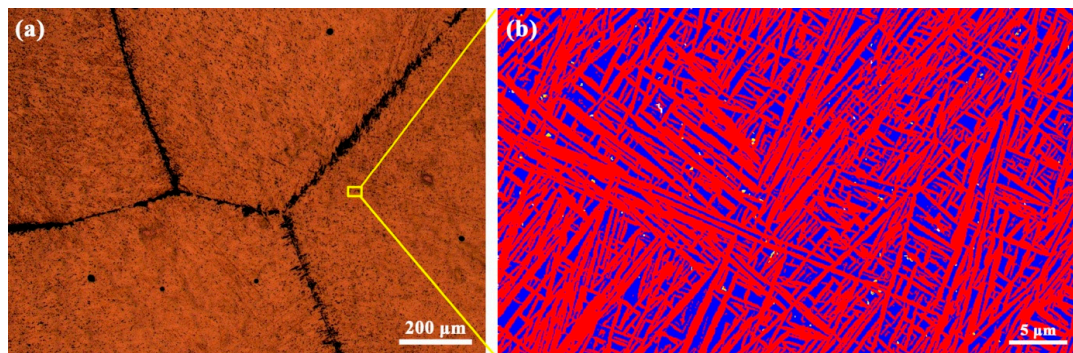

Figure 1. (**a**) OM (optical microscopic image) image of the present alloy heat-treated in β phase field followed by QC (brine-quenched); (**b**) Phase map shows the α_2' martensitic laths in the β grain interior. The blue color denotes the β matrix and the red represents the α_2' laths. The stepping size is 50 nm.

It is interesting to observe that after AC, as shown in Figure 2, the microstructure also contains numerous α_2 laths, as those under QC do. By simple comparison, one can note that, firstly, the morphology of these α_2 laths is very similar with that of the α_2' martensite shown in Figure 1. They also homogeneously nucleate inside of the β grains and form different variants. No α_2/γ lamellar colonies were produced. Secondly, by using a geometry method proposed by Pak et al. [13], we found that for both the QC and AC samples, the α_2 laths possess the same habit plane, i.e., $\{345\}_\beta$. Such a habit plane has only a ~7° deviation from that $\{11\ 11\ 13\}_\beta$ for conventional titanium alloys [14], and is quite close (~4° deviation) to the value of $\{7\ 12\ 14\}_\beta$ theoretically calculated by Mayer et al. [9] for Ti-44.58Al-3.23Mo-0.12B alloy. Thirdly, the chemical composition of AC α_2 laths only slightly differs from that of the parent β phase, as tabulated in Table 1, indicating that the transformed α_2 phase during AC is supersaturated and the diffusion process is suppressed. All this evidence demonstrates a martensitic $\beta \rightarrow \alpha_2'$ transformation during AC, despite the moderate cooling rate. However, one should note that the martensitic laths in the AC sample are much larger than those in the QC sample, probably because in the former the transformation stresses can be released in time by the recovery of the soft β matrix.

The major difference in phase constituents between QC and AC samples is that in the latter a huge number of γ laths are produced. Unlike the $\alpha \rightarrow \gamma$ transformations in normal TiAl alloys, in the present case the γ laths always nucleate at the β/α_2' interfaces and mainly grow into the β matrix, but also slightly consume the α_2' martensite, which leads to curved β/α_2' interfaces. Besides this, the chemical composition of the γ phase is quite close to that of the β matrix, as demonstrated in Table 1.
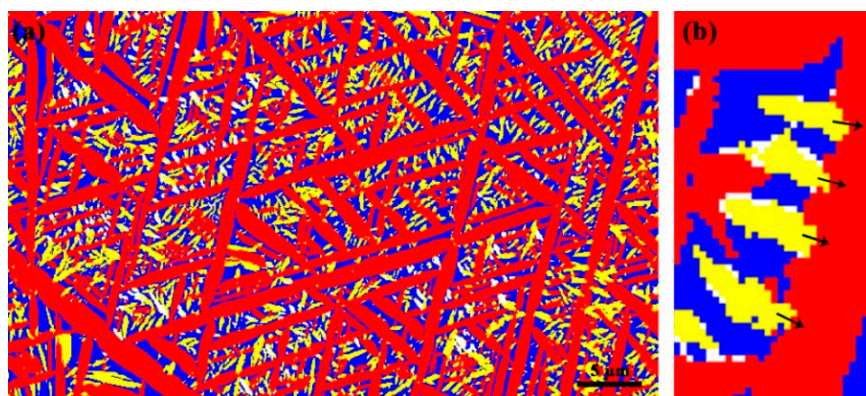
Figure 2. (**a**) Phase map of the present alloy after heat treatment in β phase field followed by AC (air-cooling). The red color is α_2', the blue is the β matrix and the yellow denotes γ phase. The step size is 50 nm; (**b**) A local part of the phase map shows the slight penetration of the γ laths into the α_2' laths, as shown by the arrows.

Table 1. Chemical composition of various phases in the AC sample by EDS (energy dispersive spectrometer).

Element	α_2'	β/B2	γ
Ti (at. %)	50.1 ± 0.7	50.2 ± 0.4	49.9 ± 0.9
Al (at. %)	39.7 ± 1.1	39.0 ± 1.5	40.2 ± 2.6
V (at. %)	10.1 ± 0.9	10.7 ± 1.0	9.8 ± 1.2

The formation of γ laths indicates an apparent β→γ transformation subsequent to the martensitic transformation, which results in the significant reduction of the β phase so that only ~28 vol. % is retained. Such a transformation can be rationalized by the simplified time–temperature–transformation (TTT) diagram shown in Figure 3. In this diagram, the high temperature *C* curve represents the β→α transformation and the two at low temperature denote the decomposition of the residual β phase and α phase into γ, respectively. Moreover, the α→γ lags behind the β→γ transition. Based on the TTT diagram, it can be speculated that in the QC condition, the β phase can be directly cooled down without any decomposition and eventually transforms into martensite, whereas in the AC condition the cooling curve can avoid the β→α transformation but passes though the β→γ region and the α→γ region to some degree.
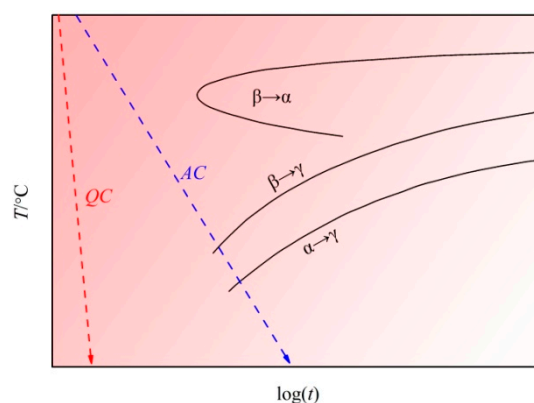

Figure 3. Schematic of TTT (time–temperature–transformation) diagram to show the decomposition pathways of β phase in V-rich TiAl alloys. The data of the map was quoted from Ref. [11]. Note that this diagram is for Ti-42Al-8V but can roughly describe the β-decomposition pathways for the present Ti-40Al-10V alloy.

3.2. Crystallography and Variant Selection

3.2.1. α_2' Martensite

Figure 4a shows a local orientation map of α_2' laths in a β grain interior for the AC sample. The corresponding pole figures in Figure 4b for the α_2' phase and β matrix indicate a Burgers OR so that $\{110\}_\beta$ // $\{00.1\}_{\alpha_2'}$ and $<111>_\beta$ // $<11.0>_{\alpha_2'}$. Such an OR results in twelve variants. Note that all the α_2' variants are detected in such a small map, shown in Figure 4a, and the corresponding variant numbers are labeled. It is interesting to note that six variants (V2, V3, V4, V6, V7 and V9) on this map are predominant whereas the others are evidently suppressed, as shown by the statistical results in Figure 5a. Simultaneously, from the map one can observe that the six major α_2' variants are intersected and form two sets of triangular configurations, as shown in Figure 4c,d, which possess very similar geometric orientations (i.e., the traces of V2, V4, V6 are parallel to those of V9, V3, V7, respectively). The pole figures shown in Figure 4d reveal that for the three variants constituting each triangular configuration, they share one common $<11.0>$ pole which is also the Burgers OR direction of the parent β phase. That is, the three variants are interrelated by a 60° rotation around the common $<11.0>$ axis. Such a configuration is believed to result from the accommodation of the transformation strain of one variant by others, and is helpful in reducing elastic energy concentration in one direction [15–17]. All of this evidence demonstrates the occurrence of local variant selection.
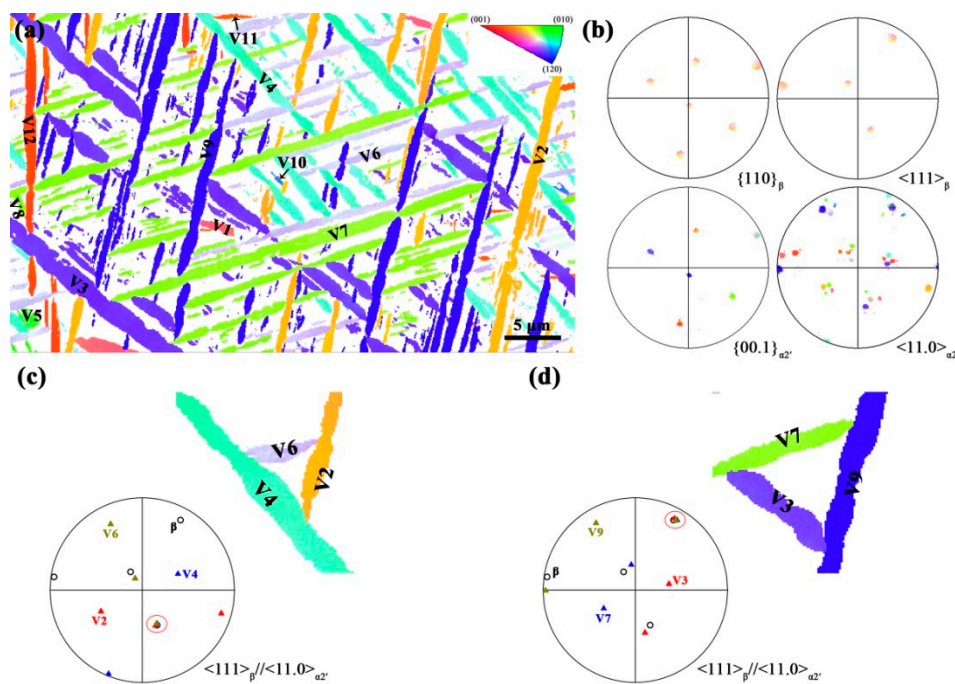

Figure 4. (**a**) The inverse pole figure map shows the orientations of different α_2' variants. The map is corresponds to Figure 2a and the variant numbers are labeled; (**b**) Pole figures for β matrix and α_2' phase, respectively. Note that a Burgers OR is evident; (**c,d**) show two triangular configurations formed by two sets of α_2' variants. For each set the three variants share a common $[11.0]_{\alpha_2'}$ axis which is also parallel to the $[111]_\beta$ direction of the matrix, as outlined by the red cycles.
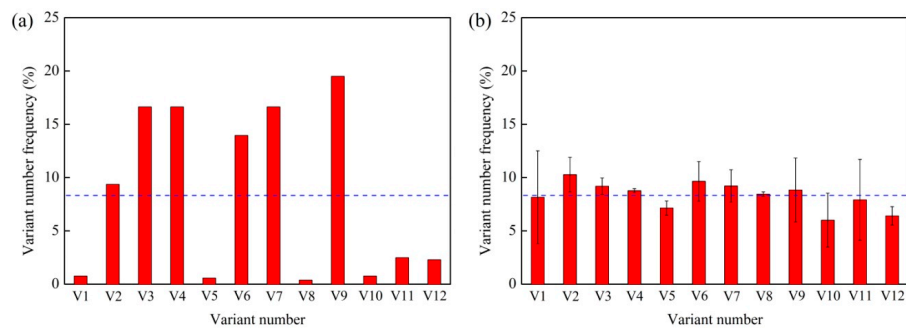
Figure 5. Statistical results of the α_2' variant number frequency for (**a**) The local map shown in Figure 4 and (**b**) three large maps with area of about $250 \times 150 \ \mu m^2$ for each.

It should be pointed out that we have examined many grains and found that the case of two-triangular-configuration is not common. In most cases there is only one triangular configuration predominant for local regions. An example is shown in Figure 6, in which one can clearly observe that there are only three major α_2' variants, i.e., V2, V4 and V6, forming a definite triangular configuration. However, we have also examined large areas and found that from a global viewpoint, there is no apparent variant selection, as shown by the statistical results in Figure 5b. Based on all the above results, it can be speculated that a parent β grain can be divided into numerous micro-domains. For each domain, three (or six) variants sharing one (or two) common $<11.0>_{\alpha_2'}//<111>_\beta$ pole(s) are predominant due to the accommodation of the transformation strain, and the formation of other variants is suppressed. Hence local variant selection exists in each domain, but there is no global variant selection.
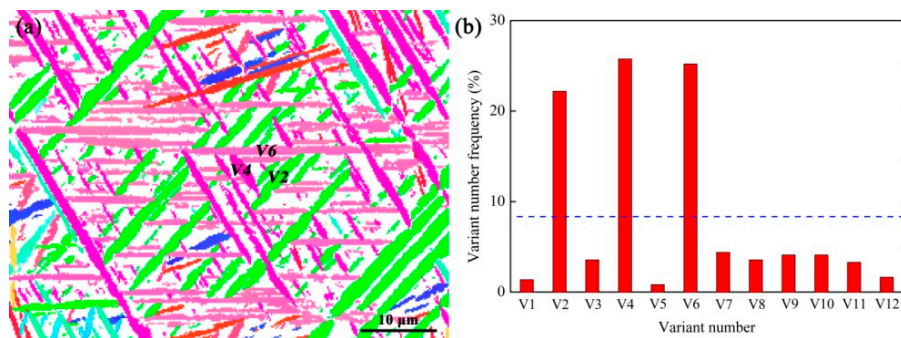

Figure 6. (**a**) The local inverse pole figure map shows that there is only one triangular configuration constituted by three α_2' variants V2, V4 and V6; (**b**) Histogram of the number frequency for the twelve variants in the map. Note that V2, V4 and V6 are predominant.

3.2.2. γ Laths

As mentioned above, numerous γ laths formed in the AC sample. These γ laths nucleated at the α_2'/β interfaces and grew mainly via $\beta \rightarrow \gamma$ decomposition. Such a transformation is believed to be diffusion-controlled because it only appeared in the AC sample rather than during QC, though the chemical composition of γ phase differs slightly from that of the β matrix, as shown in Table 1. The pole figures shown in Figure 7 indicate that there were twenty-four γ variants in total, given the fact that the γ lattice was treated as a normal FCC. Moreover, by comparing the pole figures shown in Figures 4b and 7, one can note that there is a clear Blackburn OR between the γ phase and α_2' laths, i.e., $\{111\}_\gamma//\{00.1\}_{\alpha_2'}$ and $<110>_\gamma//<11.0>_{\alpha_2'}$, and a Kurdjumov-Sachs (K-S) OR ($\{111\}_\gamma//\{110\}_\beta$ and $<110>_\gamma//<111>_\beta$) between the γ lath and β matrix as well. However, it appears that the K-S OR does not directly result from the β phase because there is no clearly-defined habit plane between β and γ phase, as one can see in a map at high magnification, as shown in Figure 8. Furthermore, locally

there are not several variants among the possible twenty-four K-S OR variants but only two: the two γ variants deriving from α_2' according to the Blackburn OR. Also, these two γ variants are twin-related and thus form twin boundaries (TB) when they are encountered. See for instance γ_1/γ_2 and γ_3/γ_4 in Figure 3b. Hence, the γ variants do not derive from β but from the α_2' and therefore the K-S OR comes from the combination of the Burgers OR and Blackburn OR, i.e., $\{110\}_\beta//\{00.1\}_{\alpha_2'}//\{111\}_\gamma$ and $<111>_\beta//<11.0>_{\alpha_2'}//<110>_\gamma$. It should be pointed out that the two γ variants derived from a given α_2' lath are roughly equal in number and thus their local number frequency is directly related to those of the α_2' variants.
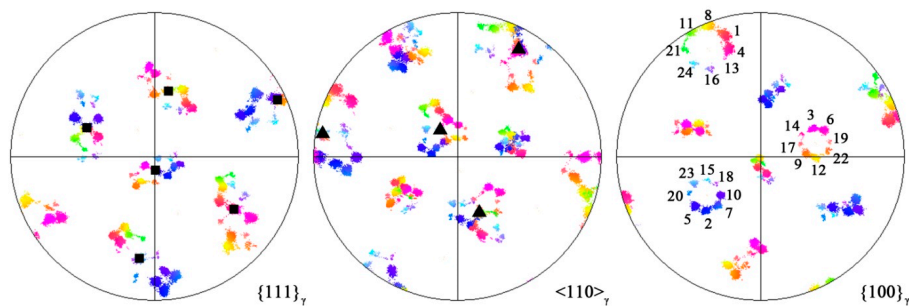

Figure 7. Pole figures for the γ phase in Figure 2a. In comparison with those in Figure 4b, a Blackburn OR and a K-S (Kurdjumov–Sachs) OR are evident. The OR-related planes/axes are marked by cubic/triangular symbols. The twenty-four γ variants are indicated in the $\{100\}_\gamma$ pole figure.
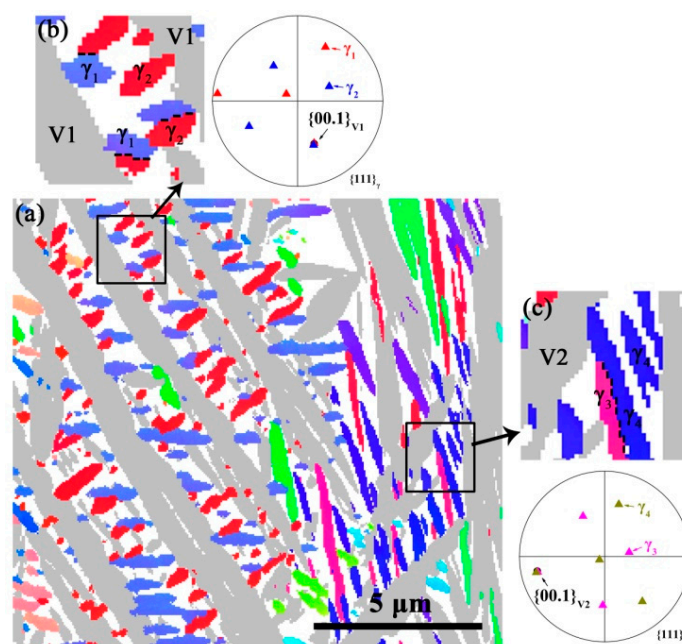

Figure 8. (**a**) The local inverse pole figure map shows the γ orientations. The α_2' phase is in gray; (**b**) and (**c**) show that the two γ variants derived from one α_2' lath are twin-related. The dash lines denote the twin boundaries. The $\{00.1\}_{\alpha_2'}$ poles are superimposed on the corresponding $\{111\}_\gamma$ pole figures.

3.3. Microstructure Decomposition during Tempering

Based on all the above results, one can note that the AC microstructure of the present alloy is mainly produced via martensitic transformation, which is thermodynamically unstable. Hence the sample was tempered to obtain a stable microstructure. After being heat-treated at 800 °C for 2 h,

as shown in Figure 9, the α_2' martensite partially decomposed into the γ phase, indicating that a $\alpha_2' \rightarrow \gamma$ transformation is evident during tempering. Such a transition can be readily clarified by the TTT diagram shown in Figure 3. Moreover, similar to during AC, one α_2' lath always produces two γ variants according to the Blackburn OR. However, the γ nuclei are mainly formed inside the α_2' laths rather than at the interfaces. After that, they grow and interlink to form large γ laths. After tempering at 1000 °C for 4 h, as shown in Figure 10a, there were very few α_2' laths retained and the volume fraction of γ phase was significantly increased from ~18% to ~54%. Moreover, the γ laths were evidently spheroid-shaped and very fine with a mean diameter of only ~0.6 μm, as shown in Figure 10b.
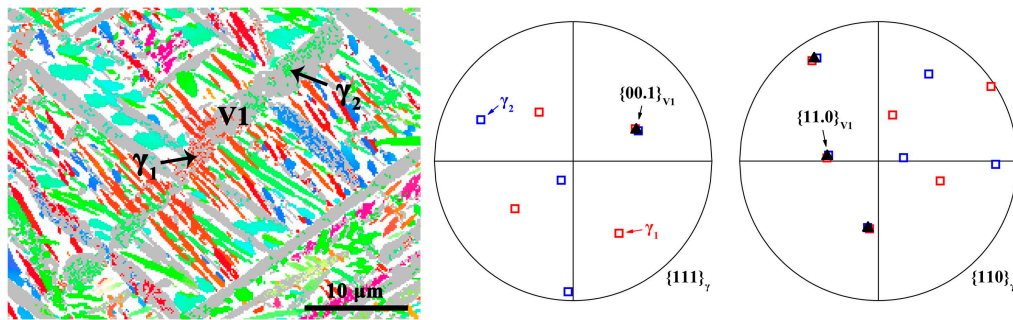

Figure 9. Microstructure of the alloy after tempering at 800 °C for 2 h. The gray color denotes the α_2' phase. The pole figures of the transformed γ phase are also presented to demonstrate the Blackburn OR with the corresponding α_2' laths.
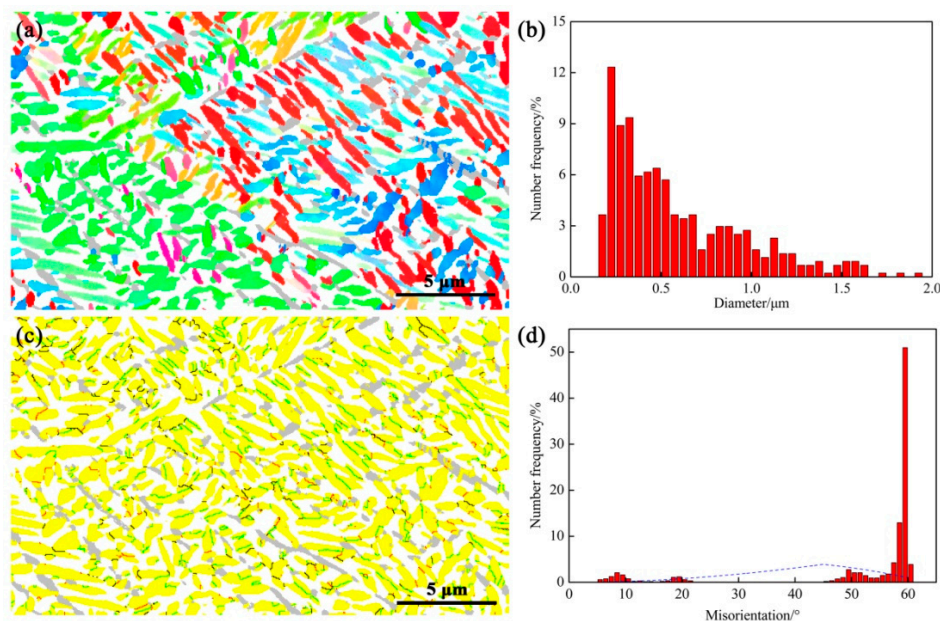

Figure 10. (**a**) Inverse pole figure map of the γ phase after tempering at 1000 °C for 4 h. The gray color denotes the retained α_2' phase; (**b**) Histogram of the γ grain diameter distribution; (**c**) γ GB (grain boundary) map. The red lines denote the low-angle GBs with $\theta < 15°$ where θ is the misorientation angle, blue lines represent GBs with $\theta \approx 60°$ and the black lines are normal high-angle GBs; (**d**) Histogram of the GBs misorientation distribution. The random distribution is represented by the dash line.

Another interesting phenomenon is that, as shown in Figure 10c,d, the grain boundary (GB) misorientation distribution shows distinctive feathering that is far from the random distribution, but exhibits strong density around 60°, as well as faint peaks at 10°, 20° and 50°. The number frequency of 60° GBs was higher than 50%. This was, as mentioned in Section 3.2.2, because each

$\alpha_2{'}$ variant can produce two γ variants and thus there are twenty-four γ variants in a single β grain. The GB (or intervariant plane) between any two γ variants is definite when they intersect. All the twenty-four γ variants can only produce ten independent misorientations, as listed in Table 2. Consequently, the misorientation angle distribution of γ phase is quantitatively different from that of the random distribution. However, such an interpretation is unsatisfactory because the predicted results are inconsistent with the measured results. For instance, the theoretical number frequency of the 60° GBs is only ~13% (see Table 2), which is much lower than the measured result (>50%). Meanwhile, in Section 3.2.2 we noted local variant selection of martensite, where in most cases three of the $\alpha_2{'}$ variants sharing a common $[11.0]_{\alpha_2{'}}$ axis were locally predominant. Because one $\alpha_2{'}$ lath simultaneously produces two twin-related γ variants, one can readily deduce that after tempering, there are six major γ variants which share a common $[110]_\beta$ axis (also the $[111]_\beta$ derived from the K-S OR) in a local region. They correspond to $\gamma_1-\gamma_6$ as shown in Table 1. One can clearly note that these variants could only form three independent misorientation angles, i.e., 10.53°, 49.47° and 60°, and the theoretical number frequencies were 20%, 20% and 60%, respectively. Such a misorientation distribution is very similar to the experimental results shown in Figure 10d. One should note that such a misorientation distribution feature is also valid from a global viewpoint, because the GB misorientation is determined by the adjacent grains, namely, the local variants. Such a GB misorientation feature may have a significant effect on the mechanical properties.

Table 2. The twenty-four γ variants derived from one β grain and the crystallographic relationships between γ_1 and other variants. The variant numbers correspond to those in Figure 7.

Specific OR with Parent β	Variant No.	Misorientation Axis/Angle between γ_1 and Other Variants
$<110>_\gamma // [111]_\beta$	γ_1	-
	γ_2	[0.577 0.577 0.577]/60°
	γ_3	[0 0.707 0.707]/60°
	γ_4	[0 $\overline{0.707}$ $\overline{0.707}$]/10.53°
	γ_5	[0 $\overline{0.707}$ $\overline{0.707}$]/60°
	γ_6	[0 0.707 0.707]/49.47°
$<110>_\gamma // [\overline{1}11]_\beta$	γ_7	[$\overline{0.577}$ $\overline{0.577}$ 0.577]/49.47°
	γ_8	[0.577 0.577 [$\overline{0.577}$]]/10.53°
	γ_9	[$\overline{0.615}$ 0.186 $\overline{0.767}$]/50.51°
	γ_{10}	[$\overline{0.739}$ $\overline{0.462}$ 0.490]/50.51°
	γ_{11}	[0.933 0.354 0.065]/14.88°
	γ_{12}	[$\overline{0.357}$ 0.603 0.714]/57.21°
$<110>_\gamma // [1\overline{1}1]_\beta$	γ_{13}	[0.354 $\overline{0.933}$ $\overline{0.065}$]/14.88°
	γ_{14}	[$\overline{0.490}$ 0.462 $\overline{0.739}$]/50.51°
	γ_{15}	[$\overline{0.738}$ $\overline{0.246}$ 0.628]/57.21°
	γ_{16}	[0.659 $\overline{0.659}$ $\overline{0.363}$]/20.61°
	γ_{17}	[$\overline{0.659}$ 0.363 $\overline{0.659}$]/51.73°
	γ_{18}	[$\overline{0.719}$ $\overline{0.302}$ 0.626]/47.11°
$<110>_\gamma // [11\overline{1}]_\beta$	γ_{19}	[$\overline{0.186}$ 0.767 0.615]/50.51°
	γ_{20}	[0.357 0.714 $\overline{0.603}$]/57.21°
	γ_{21}	[0.955 0 $\overline{0.296}$]/20.61°
	γ_{22}	[$\overline{0.302}$ 0.626 0.719]/47.11°
	γ_{23}	[0.246 $\overline{0.628}$ $\overline{0.738}$]/57.21°
	γ_{24}	[0.912 $\overline{0.410}$ 0]/21.06°

In conclusion, a β-γ microstructure was produced after tempering at 1000 °C. Such a microstructure is expected to possess superior hot workability owing to the large volume fraction of the β phase. Moreover, such a treatment, resembling the quenching-tempering in steels, may be a new strategy for microstructural design of TiAl alloys, under the premise that the β matrix is hardened

by ceramic particles such as borides, carbides or silicides to obtain a sufficiently high temperature strength. Further studies will be presented later.

4. Conclusions

The $\beta \to \alpha$ martensitic transformation has been explored in many titanium alloys, but it is very difficult to initiate in β-solidifying TiAl-based alloys. Hence the desire to understand the morphology and crystallography of martensitic transformations in TiAl alloys is impeded. Furthermore, adjusting mechanical properties by martensitic transformation, as can be done with steels, seems particularly impossible for TiAl alloys given their natural brittleness. A significant decrease in critical undercooling for martensitic transformation is required. Therefore, in this study we proposed a V-rich and Al-lean TiAl alloy, Ti-40Al-10V, to examine whether the martensitic transformation could be initiated even during air-cooling. The microstructure after heat treatment was analyzed in detail, and several conclusions are drawn below.

1. Owing to the extraordinary stability of the β phase in the Ti-40Al-10V alloy, well-developed α_2' lath martensite was produced after being heat-treated in the single β phase field followed by air cooling, rather than the common α_2/γ lamellar colonies. The martensitic morphology and crystallography were very similar to that produced during quenching, but much larger in size. The obtained α_2' laths accorded a strict Burger orientation relationship ($\{110\}_\beta //\{00.1\}_{\alpha_2'}$ and $<111>_\beta //<11.0>_{\alpha_2'}$) with the β matrix and hence a total of twelve variants were produced. Local variant selection was detected, meaning that three (six) α_2' variants sharing one (two) common [11.0] axes were predominant in a local region, while no global variant selection could be noted.

2. Subsequent to the martensitic transformation, the retained β phase decomposed via a $\beta \to \gamma$ transformation. The γ laths always nucleated at the α_2'/β interface and mainly grew into the β matrix. Each α_2' lath produced two twin-related γ variants conforming to the Blackburn orientation relationship ($\{00.1\}_{\alpha_2'} //\{111\}_\gamma$ and $<11.0>_{\alpha_2'} //<110>_\gamma$). Hence there were twenty-four γ variants for a given β grain, according to a K-S orientation relationship ($\{110\}_\beta //\{111\}_\gamma$ and $<111>_\beta //<110>_\gamma$) as a result of the combination of the Burgers and Blackburn orientation relationships.

3. During tempering, the air-cooled microstructure decomposed mainly via an $\alpha_2' \to \gamma$ transformation according to the Blackburn orientation relationship. The martensite was almost completely decomposed after tempering at 1000 °C for 4 h. The volume fraction of the γ phase was significantly increased and became homogenous with sizes of about 0.5 μm. Meanwhile, due to the local variant selection, the misorientation angle distribution of the γ grain boundaries presented only several independent misorientations. Such a treatment, resembling the quenching-tempering in steels, may be a new strategy for the microstructural design of TiAl alloys.

Author Contributions: Yi Chen prepared the materials, carried out the EBSD investigations, and wrote the manuscript. Liang Cheng conceived and designed the experiments, carried out the heat-treatments, analyzed the experimental data, wrote and revised the manuscript. Lingyan Sun, Yalin Lu, Guang Yang and Hongchao Kou discussed the data. Emmanuel Bouzy revised the manuscript and discussed the results.

References

1. Appel, F.; Paul, J.D.H.; Oehring, M. *Gamma Titanium Aluminide Alloys: Science and Technology*; Wiley-VCH: Weinheim, Germany, 2011.

2.　Clemens, H.; Mayer, S. Design, processing, microstructure, properties, and applications of advanced intermetallic TiAl alloys. *Adv. Eng. Mater.* **2013**, *15*, 191–215. [CrossRef]

3.　Clemens, H.; Wallgram, W.; Kremmer, S.; Güther, V.; Otto, A.; Bartels, A. Design of novel β-Solidifying TiAl alloys with adjustable β/B2-phase fraction and excellent hot-workability. *Adv. Eng. Mater.* **2008**, *10*, 707–713. [CrossRef]

4.　Ahmed, T.; Rack, H.J. Phase transformations during cooling in α + β titanium alloys. *Mater. Sci. Eng. A* **1998**, *243*, 206–211. [CrossRef]

5.　Beladi, H.; Chao, Q.; Rohrer, G.S. Variant selection and intervariant crystallographic planes distribution in martensite in a Ti–6Al–4V alloy. *Acta Mater.* **2014**, *80*, 478–489. [CrossRef]

6.　Yang, G.; Kou, H.C.; Yang, J.R.; Li, J.S.; Fu, H.Z. Microstructure control of Ti-45Al-8.5Nb–(W,B,Y) alloy during the solidification process. *Acta Mater.* **2016**, *112*, 121–131. [CrossRef]

7.　Yamabe, Y.; Takeyama, M.; Kikuchi, M. Microstructure evolution through solid-solid phase transformations in gamma titanium aluminides. In *Gamma Titanium Aluminides*; Kim, Y.W., Wagner, R., Yamaguchi, M., Eds.; TMS: Warrendale, PA, USA, 1995; pp. 111–129.

8.　Hu, D.; Jiang, H. Martensite in a TiAl alloy quenched from beta phase field. *Intermetallics* **2015**, *56*, 87–95. [CrossRef]

9.　Mayer, S.; Petersmann, M.; Fischer, F.D.; Clemens, H.; Waitz, T.; Antretter, T. Experimental and theoretical evidence of displacive martensite in an intermetallic Mo-containing γ-TiAl based alloy. *Acta Mater.* **2016**, *115*, 242–249. [CrossRef]

10.　Appel, F.; Clemens, H.; Fischer, F.D. Modeling concepts for intermetallic titanium aluminides. *Prog. Mater. Sci.* **2016**, *81*, 55–124. [CrossRef]

11.　Takeyama, M.; Kobayashi, S. Physical metallurgy for wrought gamma titanium aluminides: Microstructure control through phase transformations. *Intermetallics* **2005**, *13*, 993–999. [CrossRef]

12.　Zambaldi, C.; Zaefferer, S.; Wright, S.I. Characterization of order domains in γ-TiAl by orientation microscopy based on electron backscatter diffraction. *J. Appl. Crystallogr.* **2009**, *42*, 1092–1101. [CrossRef]

13.　Pak, H.R.; Chang, S.N.; Kato, M. A new method of determining the orientation of the parent phase and the habit plane normal. *J. Mater. Sci.* **1985**, *20*, 947–954. [CrossRef]

14.　Bhattacharyya, D.; Viswanathan, G.B.; Denkenberger, R.; Furrer, D.; Fraser, H.L. The role of crystallographic and geometrical relationships between α and β phases in an α/β titanium alloy. *Acta Mater.* **2003**, *51*, 4679–4691. [CrossRef]

15.　Balachandran, S.; Kashiwar, A.; Choudhury, A.; Banerjee, D.; Shi, R.; Wang, Y. On variant distribution and coarsening behavior of the α phase in a metastable β titanium alloy. *Acta Mater.* **2016**, *106*, 374–387. [CrossRef]

16.　Hua, K.; Zhang, Y.D.; Kou, H.C.; Li, J.S.; Gan, W.M.; Fundenberger, J.J.; Esling, C. Composite structure of α phase in metastable β Ti alloys induced by lattice strain during β to α phase transformation. *Acta Mater.* **2017**, *132*, 307–326. [CrossRef]

17.　Sankaran, A.; Bouzy, E.; Humbert, M.; Hazotte, A. Variant selection during nucleation and growth of γ-massive phase in TiAl-based intermetallic alloys. *Acta Mater.* **2009**, *57*, 1230–1242. [CrossRef]